# An Optimal Energy Storage Control Strategy for Grid-connected Microgrids

Pawel Malysz, *Member, IEEE*, Shahin Sirouspour, *Member, IEEE*, and Ali Emadi, *Fellow, IEEE*

***Abstract*—This paper presents an online optimal energy/power control method for the operation of energy storage in grid-connected electricity microgrids. The approach is based on a mixed-integer-linear-program optimization formulated over a rolling horizon window, considering predicted future electricity usage and renewable energy generation. Performance objectives include electricity usage cost, battery operation costs, and utility oriented goals related to the peak demand and load smoothing. A robust counterpart formulation of the optimization problem is also proposed to handle uncertainty in energy demand/generation prediction in a computationally efficient way. Further reduction in the computations is achieved by employing variable time steps and relaxing binary constraints. A series of simulations demonstrate the effectiveness of various features of the proposed energy/power management methodology in different scenarios.**

***Index Terms*—Adaptive control, battery, energy management, microgrid, mixed integer linear programming, robust optimization, rolling horizon, smartgrid, solar power, wind power.**

## Glossary of Terms and Nomenclature

### A. Constants

| | |
|---|---|
| $N_h \in \mathbb{Z}$ | Number of time steps in horizon. |
| $\mathbf{h} \in \Re^{N_h}$ | Vector of time step lengths in hours. |
| $E_{\text{bat}}^{\min} \in \Re$ | Minimum battery energy level. |
| $E_{\text{bat}}^{\max} \in \Re$ | Maximum battery energy level. |
| $P_{\text{bat}}^{\text{loss}} \in \Re$ | Battery self-discharge power loss. |
| $\eta_c \in \Re$ | Battery charging efficiency. |
| $\eta_d \in \Re$ | Battery discharging efficiency. |
| $p_{\text{bat}}^{gc,\max} \in \Re$ | Max battery green zone charging rate. |
| $p_{\text{bat}}^{rc,\max} \in \Re$ | Max red zone incremental charging rate. |
| $p_{\text{bat}}^{gd,\max} \in \Re$ | Max battery green zone discharging rate. |
| $p_{\text{bat}}^{rd,\max} \in \Re$ | Max red zone incremental discharging rate. |
| $\Delta p_{\text{bat}} \in \Re$ | Max change in battery power rate. |
| $T^{\text{maxon}} \in \Re$ | Red zone maximum on-time in hours. |
| $T^{\text{minoff}} \in \Re$ | Red zone minimum off-time in hours. |
| $\Gamma \in \Re$ | Polyhedral set size robustness parameter. |
| $\lambda \in \Re$ | Battery capacity fade factor, $0 \ll \lambda < 1$. |

### B. Rolling Horizon Control Variables

| | |
|---|---|
| $\mathbf{c}_{\text{buy}} \in \Re^{N_h}$ | Electricity usage buying cost. |
| $\mathbf{c}_{\text{sell}} \in \Re^{N_h}$ | Electricity selling price. |
| $c_{\text{peak}} \in \Re$ | Peak electricity demand usage cost. |
| $\mathbf{c}_{\text{batg}} \in \Re^{N_h}$ | Battery usage cost for green zone rates. |
| $\mathbf{c}_{\text{batr}} \in \Re^{N_h}$ | Battery usage cost for red zone rates. |
| $\mathbf{c}_{smb} \in \Re^{N_h}$ | Battery signal smoothing penalty. |
| $\mathbf{c}_{smg} \in \Re^{N_h}$ | Grid signal smoothing penalty. |
| $c_{\text{flat}} \in \Re$ | Grid signal flattening penalty. |
| $E_{\text{bat}}^{o} \in \Re$ | Actual battery energy at start of horizon. |
| $E_{\text{bat}}^{\text{final}} \in \Re$ | Desired battery energy at end of horizon. |
| $p_g^{\text{base}} \in \Re$ | Baseline for demand charges in horizon. |
| $\bar{\mathbf{p}}_d \in \Re^{N_h}$ | Estimate of predicted net demand. |
| $\Delta\bar{\mathbf{p}}_d \in \Re^{N_h}$ | Error estimate of predicted net demand. |
| $\mathbf{P}_s^{d_b\,\max} \in \Re^{N_h x N_h}$ | Diagonal matrix of upper bounds. |
| $\mathbf{P}_s^{d_u\,\max} \in \Re^{N_h x N_h}$ | Diagonal matrix of upper bounds. |
| $\mathbf{P}_s^{c_s\,\max} \in \Re^{N_h x N_h}$ | Diagonal matrix of upper bounds. |
| $\mathbf{P}_s^{c_u\,\max} \in \Re^{N_h x N_h}$ | Diagonal matrix of upper bounds. |

### C. Optimization Variables

| | |
|---|---|
| $\mathbf{p}_s^{c_s} \in \Re^{N_h}$ | Storage charging rate (offset selling portion). |
| $\mathbf{p}_s^{c_u} \in \Re^{N_h}$ | Storage charging rate (uncertain portion). |
| $\mathbf{p}_s^{c_b} \in \Re^{N_h}$ | Storage charging rate (grid buying portion). |
| $\mathbf{p}_s^{d_b} \in \Re^{N_h}$ | Storage discharging rate (offset buying portion). |
| $\mathbf{p}_s^{d_u} \in \Re^{N_h}$ | Storage discharging rate (uncertain portion). |
| $\mathbf{p}_s^{d_s} \in \Re^{N_h}$ | Storage discharging rate (grid selling portion). |
| $\mathbf{p}_{\text{bat}}^{gc} \in \Re^{N_h}$ | Green zone battery charging power rate. |
| $\mathbf{p}_{\text{bat}}^{rc} \in \Re^{N_h}$ | Incremental red zone battery charging power rate. |
| $\mathbf{p}_{\text{bat}}^{gd} \in \Re^{N_h}$ | Green zone battery discharging power rate. |

Manuscript received May 17, 2013; revised July 17, 2013, August 20, 2013, October 29, 2013, December 14, 2013; accepted January 19, 2014. Date of current version June 18, 2014. This work was supported by the Canada Excellence Research Chairs Program. Paper no. TSG-00403-2013.

P. Malysz is with the McMaster Institute for Automotive Research and Technology (MacAUTO), McMaster University, Hamilton, ON L8S 4K1, Canada (e-mail: malyszp@mcmaster.ca).

S. Sirouspour is with the Department of Electrical and Computer Engineering, McMaster University, Hamilton, ON L8S 4K1, Canada (e-mail: sirouspour@ece.mcmaster.ca).

A. Emadi is with the McMaster Institute for Automotive Research and Technology (MacAUTO), and also with the Departments of Mechanical Engineering, and Electrical and Computer Engineering, McMaster University, Hamilton, ON L8S 4K1, Canada (e-mail: emadi@mcmaster.ca).

Digital Object Identifier 10.1109/TSG.2014.2302396

| | |
|---|---|
| $\mathbf{p}_{\text{bat}}^{rd} \in \Re^{N_h}$ | Incremental red zone battery discharging rate. |
| $\mathbf{u}_g \in \Re^{N_h}$ | Auxiliary vector for grid signal smoothing. |
| $\mathbf{u}_b \in \Re^{N_h}$ | Auxiliary vector for battery signal smoothing. |
| $p_g^{ob} \in \Re$ | Maximum net power demand over some baseline. |
| $p_g^{\max} \in \Re$ | Maximum net power demand. |
| $p_g^{\min} \in \Re$ | Minimum net power demand. |
| $\boldsymbol{\delta}_{bs1} \in \mathbb{Z}^{N_h}$ | Binary vector for buying/uncertain/selling states. |
| $\boldsymbol{\delta}_{bs2} \in \mathbb{Z}^{N_h}$ | Binary vector for buying/uncertain/selling states. |
| $\boldsymbol{\delta}_{cd} \in \mathbb{Z}^{N_h}$ | Binary vector for battery charging/discharging. |
| $\boldsymbol{\delta}_r \in \mathbb{Z}^{N_h}$ | Binary vector for battery red-zone rate usage. |
| $t \in \Re$ | Auxiliary variable used to minimize worst case. |
| $z_c \in \Re$ | Robust counterpart auxiliary variable. |
| $z_d \in \Re$ | Robust counterpart auxiliary variable. |
| $\mathbf{w}_c \in \Re^{N_h}$ | Robust counterpart auxiliary vector. |
| $\mathbf{w}_d \in \Re^{N_h}$ | Robust counterpart auxiliary vector. |

## I. Introduction

MICROGRIDS will play a critical role in an organic transformation of the existing electricity grid to the smart grid of future. They can help integrate distributed renewable energy generation and storage capacity to the grid to enhance its reliability and reduce reliance on carbon-emitting fossil fuels for power generation. Microgrids can be instrumental in supporting deep penetration of plug-in electric vehicles (P-EVs) and plug-in hybrid electric (P-HEV) vehicles. Power and energy management is an important aspect of microgrid control systems and has been a subject of significant ongoing research [1]–[3].

Offline optimization-based scheduling approaches are popular for use in energy management systems (EMS); they can improve system efficiency and meet multiple system goals using well known optimization algorithms. Deng *et al.* [4] proposed multi-objective offline scheduling to satisfy both economic and emission reduction objectives for microgrid management employing photo-voltaic arrays, wind turbines, battery storage, fuel cell, and micro turbine. They employed a multi-objective genetic algorithm to solve the resulting optimization problem. Mohamed and Koivo [5] formulated a nonlinear multi-objective offline optimization based strategy for management of an isolated electric only microgrid consisting of wind turbine, PV cells, battery storage, micro turbine, diesel generator and fuel cell; their goals were minimization of costs and emissions. Levron *et al.* [6] proposed a dynamic programming offline scheduling approach for operation of a grid-connected micro grid with multilevel objectives such as voltage/current limits and network topology. Moghaddam *et al.* [7] employed a multi-objective adaptive modified particle swarm optimization for management of micro grids with renewable energy and backup hybrid turbine/fuel-cell/battery power; the optimization problem in this work is nonlinear. Mohammadi *et al.* [8] proposed a robust optimization scheduling approach using the point estimate method for management of microgrids with storage and renewable energy sources; they considered uncertainty in generation and prices.

Linear programming has been very popular for offline scheduling and optimization since economic goals can often be expressed as linear functions of the decision variables. Many standard solvers exist for linear programming problems. Kim and Kinoshita [9] employed offline linear programming to make electricity buying/selling decisions in microgrids. Chakraborty *et al.* [10] proposed a high-frequency AC microgrid with battery storage and solar/wind power. Their distributed intelligent energy management system is based on a day ahead non-robust linear program economic based optimization. Morais *et al.* [11] introduced an offline nonrobust optimization for power dispatch control using mixed-integer-linear-program (MILP); they considered an electric only microgrid with PV panels, wind turbine, fuel cell, battery storage, and controllable load. Tsikalakis and Hatziargyriou [12] proposed a centralized economic based optimization for electricity production and load shedding decisions in a microgrid using an offline nonrobust MILP formulation. Chaouachi *et al.* [13] scheduled battery usage using a multi-objective linear program with fuzzy-logic to handle uncertainties in forecasted parameters. Handschin *et al.* [14] presented an offline stochastic optimization-based MILP to robustly schedule the power dispatching in a microgrid. The robustness in their approach, however, comes at the expense of greatly increasing the size of the MILP optimization problem.

Online model predictive control (MPC) or rolling horizon control approaches have also been proposed for microgrid management. In these methods, an optimization problem is formulated and solved over a rolling window at each time step. In [15], Ulbig *et al.* proposed a cascaded nonrobust MPC framework in which MPCs operate at multiple layers on different time-scales. Each layer is designated to control certain aspects of the system, ranging from high-level grid planning objectives, mid-level heat/power dispatch, to low level objectives such as voltage control. Molderink *et al.* [16] presented a simple nonrobust MILP-based MPC for microgrids with both heat/cold storage and electricity storage; their optimization focuses on economic costs and balancing energy flows. Hovgaard *et al.* [17] introduced a robust MPC employing a linear optimization problem with probabilistic constraints for combined heat and power (CHP) microgrids. Their system uses heat/cold storage as opposed to electric storage; moreover their formulation leads to a nonlinear second-order cone equivalent robust counterpart problem. Parisio and Glielmo [18] formulated a nonrobust MILP optimization for their MPC with only economic savings goals. Peters *et al.* [19] studied a nonrobust MPC, employing a nonlinear optimization for an islanded forward operating base with battery storage, diesel and renewable power generation, and auxiliary plugin electric vehicle storage. Brendtsen *et al.* [20] proposed a hierarchical three-level approach for resource distribution; they employed quadratic optimization in a nonrobust MPC framework in the highest two levels of their controller. All of online methods reviewed above have employed fixed time step horizons in their optimization routines.

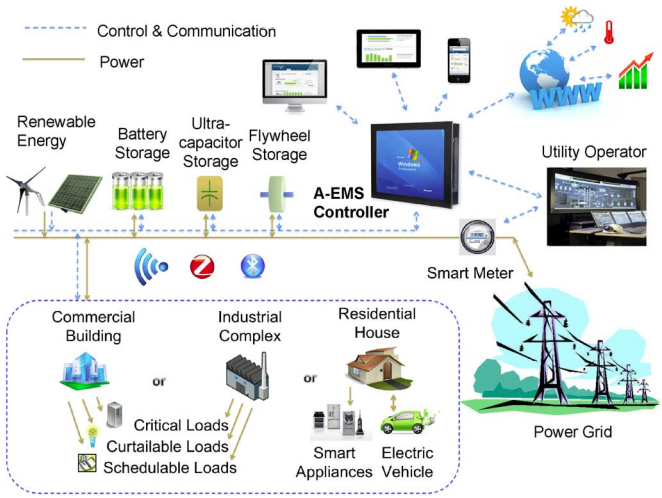


Fig. 1. Grid-connected microgrid with on-site energy storage and A-EMS controller.

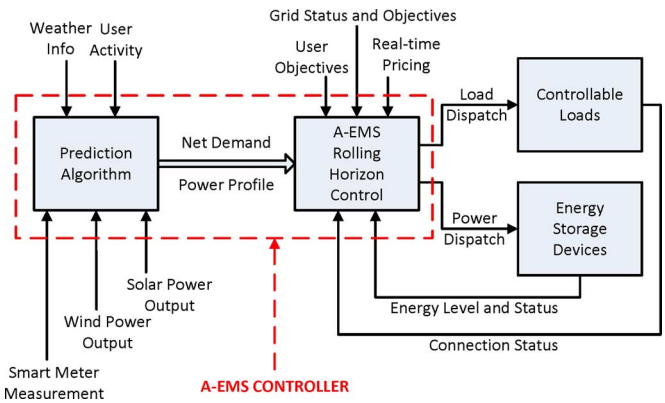


Fig. 2. Control system overview of the A-EMS with inputs and outputs.

This paper is concerned with developing optimal control strategies for power flow in grid-connected microgrids with energy storage devices, e.g., see Fig. 1. The microgrid of interest would be connected to the electricity grid and may feed a residential, commercial, or industrial load. It must have at least one electric energy storage device, e.g., a battery pack, and may also include renewable energy production, e.g., solar or wind. The adaptive energy management system (A-EMS) is proposed as a high-level controller to make optimal power flow decisions by solving a versatile multiple-objective *robust* MILP optimization problem formulated over a rolling horizon prediction window. The A-EMS communicates with all elements of the microgrid and has access to external information on weather forecasts and market electricity prices. A control block diagram for the microgrid with the A-EMS is given in Fig. 2. The goals of the A-EMS in making power flow decisions are multifaceted, ranging from economic benefits for consumers, microgrid power profile shaping for utilities, to extending battery/storage life.

A microgrid with energy storage and the A-EMS controller would provide electricity customers and utilities with economic and grid stability benefits without a need for change in the customer electricity usage habits. The A-EMS can provide demand response functionality in a way that is transparent to the customer. It does so by taking advantage of energy storage devices

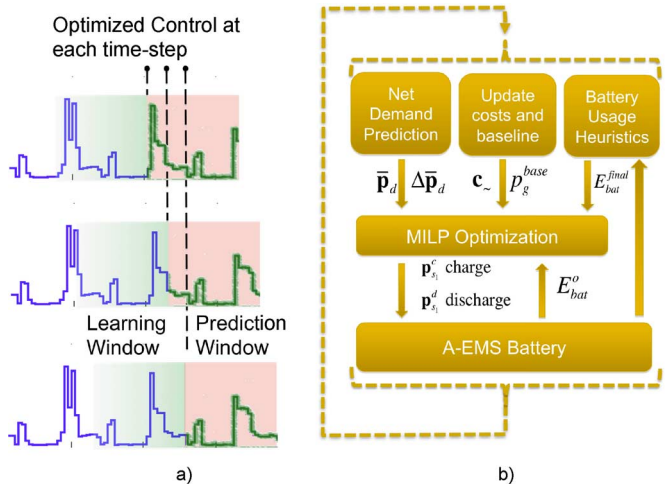


Fig. 3. Rolling horizon control. (a) Rolling window concept. (b) Block diagram.

and renewable sources of power to reduce the demand on the grid at critical times. Utilities can discourage electricity usage at peak time through a time-of-use pricing scheme, to which the A-EMS controller would respond by using local resources without the need for load curtailment. The A-EMS adaptively make decisions about energy storage usage, considering the future demand and based on several user and utility defined cost objectives.

A MILP multi-objective optimization approach is chosen for making power/energy management decisions to systematically find the best tradeoff among multiple objectives in the operation of a microgrid, while respecting the system operational constraints. The use of integer variables in this approach helps take into account charging/discharging inefficiencies, and asymmetric buying/selling prices, and allows for discrete decision variables with respect to controllable loads. At its core, MILP involves solving many linear optimization programs. Efficient and fast algorithms do exist for solving such linear programming problems, which are suitable for implementation on embedded computers. A rolling horizon control approach, depicted in Fig. 3, can use the most up-to-date predictions and latest information about the system to adapt to new events and operating conditions on the fly. This would not be feasible using offline scheduling approaches. The scope of this paper is limited to the design of the rolling horizon control block in Fig. 2 for a microgrid with controllable energy storage devices.

The proposed controller has several novel aspects compared to relevant prior work in the literature. A unique form of the cost objective considers microgrid power demand shaping objectives and storage/battery operation costs, in addition to the conventional electricity usage costs. The new concepts of battery green zone power rates and red zone incremental power rates are introduced and used in the formulation of the optimization problem. The battery can sustain continuous charging/discharging at the green zone power rates. In entering the red zones, the battery can temporarily exceed these limits subject to maximum on-time and minimum-off time constraints. Red-zone power rates can, for example, be particularly helpful in reducing peak demand costs by allowing the battery to temporarily operate outside its normal ratings in order to reduce

the peak demand. A novel *robust* formulation of the MILP optimization is proposed which takes into account prediction error bounds on future net electricity demand. This is achieved with a modest increase in computations by maintaining the MILP form of the problem and employing box and polyhedral uncertainty sets [21]. In contrast, other approaches such as probabilistic constraints or stochastic robust optimization methods substantially increase computational cost either by significantly increasing the number of variables or converting the problem to nonlinear robust counterpart problems, e.g., second-order cone. The optimization problem formulation and its solution are guided by the goal of reducing the computations so the controller can be implemented on a cost-effective embedded computer. In addition to the novel robust formulation of the optimization problem, other innovative measures such as using a variable time step length in the rolling horizon window and relaxation of binary constraints in future prediction steps help further reduce computation time.

The rest of the paper is structured as follows. A nonrobust MILP optimization formulation of rolling horizon control for energy management with storage is described in Section II. This is followed by a robust MILP optimization formulation of the problem in Section III. Simulation results highlighting different aspects of the controller are presented in Section IV. The paper is concluded in Section V.

## II. MILP Optimization-Based Rolling Horizon Energy Management

The A-EMS control algorithm employs a rolling prediction horizon or window at each time step to make power flow decisions. A block diagram of this controller is depicted in Fig. 3. It is assumed here that a prediction algorithm generates an estimated net demand power vector $\bar{\mathbf{p}}_d$ along with a bounded uncertainty error estimate $\Delta\bar{\mathbf{p}}_d$ for each future time step in the horizon. The prediction algorithm is beyond the scope of the present paper and will be reported in a future publication. A MILP optimization problem is formulated and solved at each time step to obtain optimal values for charge/discharge rates of the storage elements over the prediction horizon; only the solution for the first time step in the window is implemented in practice. In this section a nonrobust formulation of the optimization problem is presented for the case where net demand can be perfectly predicted, i.e., $\bar{\mathbf{p}}_d = \mathbf{p}_d$. The net demand vector is defined as the difference between the electricity usage of the loads and the renewable energy sources power output, i.e., $\mathbf{p}_d = \mathbf{p}_{\text{Loads}} - \mathbf{p}_{\text{Solar}} - \mathbf{p}_{\text{Wind}}$.

While the proposed algorithm is applicable to any type of storage device, this paper assumes microgrids with battery storage. A discrete-time battery model of the form

$$E_{k+1} = E_k + \eta_c \mathbf{h}_k \mathbf{p}^c_{\text{bat}_k} - \eta_d^{-1} \mathbf{h}_k \mathbf{p}^d_{\text{bat}_k} - P^{\text{loss}}_{\text{bat}} \mathbf{h}_k \qquad (1)$$

is employed here, where $E_k$ is the energy in the battery at time step $k$ typically measured in kWh, $\mathbf{h}_k$ is the length of each time step in the prediction horizon measured in hours, $P^{\text{loss}}_{\text{bat}}$ is a self discharge loss expressed as kW per hour, $\mathbf{p}^c_{\text{bat}_k}$ and $\mathbf{p}^d_{\text{bat}_k}$ are the battery charging and discharging power, $\eta_c$ and $\eta_d$ are charging and discharging efficiencies, respectively. The rolling horizon control update rate is dictated by $\mathbf{h}_1$, i.e., the first element of horizon time step duration vector $\mathbf{h}$. It is often desirable to employ a battery usage cost in the optimization to avoid unnecessary battery activity that would otherwise reduce battery life; this usage cost can be expressed in units of ¢/kWh. A simple way to estimate this cost is by assuming a half-life behavior such that the capacity of the battery drops by some multiplicative factor after each cycle. Using such a model the total life or energy throughput can be calculated using an infinite geometric series formula, i.e., $C_0\lambda/(1-\lambda)$ where $\lambda < 1$ is capacity factor loss per cycle and $C_0$ is the initial capacity. If $Bcost$ is the capital cost of the energy storage device, then the usage cost is $(Bcost(1-\lambda))/(C_0\lambda)$.

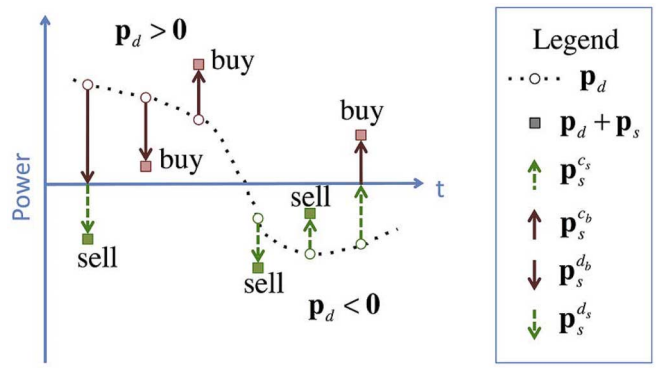


Fig. 4. Possible grid buy/sell outcomes for different storage control actions $\mathbf{p}_s = \mathbf{p}_s^{c_s} + \mathbf{p}_s^{c_b} - \mathbf{p}_s^{d_b} - \mathbf{p}_s^{d_s}$. Up arrows indicate battery charging; down arrows battery discharging.

The charge/discharge control decisions are made with the objective of minimizing the following multi-term cost function:

$$\min \Big( \cancel{\mathbf{c}_{bs}^T \mathbf{p}_d} + \mathbf{c}_{\text{sell}}^T \mathbf{p}_s^{c_s} + \mathbf{c}_{\text{buy}}^T \mathbf{p}_s^{c_b} - \mathbf{c}_{\text{buy}}^T \mathbf{p}_s^{d_b} - \mathbf{c}_{\text{sell}}^T \mathbf{p}_s^{d_s} \qquad (2a)$$

$$+ \mathbf{c}_{\text{batg}}^T \left( \mathbf{p}_{\text{bat}}^{gc} + \mathbf{p}_{\text{bat}}^{gd} \right) + \mathbf{c}_{\text{batr}}^T \left( \mathbf{p}_{\text{bat}}^{rc} + \mathbf{p}_{\text{bat}}^{rd} \right) + \mathbf{c}_{smb}^T \mathbf{u}_b \qquad (2b)$$

$$+ \mathbf{c}_{smg}^T \mathbf{u}_g + c_{\text{peak}} p_g^{ob} + c_{\text{flat}} \left( p_g^{\max} - p_g^{\min} \right) \Big). \qquad (2c)$$

All the variables in this cost function are vectors of length $N_h$, where $N_h$ is the number of steps in the rolling horizon window. The sum of terms in (2a) represent the net electricity usage cost where $\mathbf{p}_s^{c_s}$ is the portion of battery charging power to offset any negative net demand grid selling, $\mathbf{c}_{\text{sell}}$ is the electricity selling price, $\mathbf{p}_s^{c_b}$ is the portion of battery charging power which is bought from the grid, $\mathbf{c}_{\text{buy}}$ is the electricity buying price, $\mathbf{p}_s^{d_b}$ is battery discharging power to offset any positive net demand grid buying, and $\mathbf{p}_s^{d_s}$ is the portion of battery discharging power which is sold to the grid. Different possible cases of storage activity and net demand are illustrated in Fig. 4; it is seen that when $\mathbf{p}_d > 0$ then $\mathbf{p}_s^{c_s} = 0$, and when $\mathbf{p}_d < 0$ then $\mathbf{p}_s^{d_b} = 0$. The cost vector $\mathbf{c}_{bs}$ has elements equal to the price of buying or selling electricity, i.e., $\mathbf{c}_{bs_k} = \mathbf{c}_{\text{buy}_k}$ when $\mathbf{p}_{d_k} > 0$ and $\mathbf{c}_{bs_k} = \mathbf{c}_{\text{sell}_k}$ when $\mathbf{p}_{d_k} \leq 0$. The time varying electricity price can be known *a priori*, for example time-of-use rates offered by an electricity retailer. The term $\mathbf{c}_{bs}^T \mathbf{p}_d$ is the usage cost assuming zero battery activity. Since this term is not affected by the optimization decision variables it can be eliminated from the cost

function; the remaining four terms in (2a) represent electricity usage cost-savings/extra-profit.

The terms in (2b) represent battery usage costs and a battery signal smoothing term. So called green zone power limits are defined within which the battery charge/discharge rates can always lie; the vectors $\mathbf{p}_{\text{bat}}^{gc}$ and $\mathbf{p}_{\text{bat}}^{gd}$ represent the *green zone power rates* for charging and discharging, and $\mathbf{c}_{\text{batg}}$ is the cost of battery operation in the green zone. The battery power rate can also be temporarily increased beyond these limits via so called *incremental red zone power rates* denoted by vectors $\mathbf{p}_{\text{bat}}^{rc}$ and $\mathbf{p}_{\text{bat}}^{rd}$ for charging and discharging, respectively; the cost of operation in the red zone is denoted by $\mathbf{c}_{\text{batr}}$. These vectors are related to the buying/selling storage power vectors via the equality constraints

$$\mathbf{p}_s^{c_s} + \mathbf{p}_s^{c_b} = \mathbf{p}_{\text{bat}}^{gc} + \mathbf{p}_{\text{bat}}^{rc}, \quad \mathbf{p}_s^{d_b} + \mathbf{p}_s^{d_s} = \mathbf{p}_{\text{bat}}^{gd} + \mathbf{p}_{\text{bat}}^{rd}. \quad (3)$$

Note that additional storage elements (e.g., other batteries, flywheels, ultra capacitors) can be easily incorporated into the problem formulation by adding their corresponding power terms to the right-hand sides of (3). The term $\mathbf{u}_b$ represents the magnitude of the change in successive horizon time-step battery power rates and $c_{smb}$ is the cost associated with such changes; it is used to smooth the battery power profile signal.

Grid signal shaping cost/penalty terms are given in (2c). The term $\mathbf{c}_{smg}^T \mathbf{u}_g$ smooths the grid signal by minimizing successive differences in the power grid signal $\mathbf{p}_g = \mathbf{p}_s^{c_s} + \mathbf{p}_s^{c_b} - \mathbf{p}_s^{d_b} - \mathbf{p}_s^{d_s} + \mathbf{p}_d$. The middle term $c_{\text{peak}} p_g^{ob}$ represents incremental peak usage costs above the baseline $p_g^{\text{base}}$ to enable peak shaving. The last term in (2c) is meant for flattening or squeezing of the grid signal $\mathbf{p}_g$.

*1) State Decision Constraints:* The optimization in the rolling horizon controller makes decisions as to whether charge or discharge the battery storage device at given time. To this end, the following constraints are imposed on the battery power rate variables:

$$\mathbf{0} \le \mathbf{p}_{\text{bat}}^{\gamma c} \le p_{\text{bat}}^{\gamma c,\max} \boldsymbol{\delta}_{cd} \quad (4)$$

$$\mathbf{0} \le \mathbf{p}_{\text{bat}}^{\gamma d} \le p_{\text{bat}}^{\gamma d,\max} (\mathbf{1} - \boldsymbol{\delta}_{cd}) \quad (5)$$

where $\gamma = r$ or $g, \mathbf{0} \le \boldsymbol{\delta}_{cd} \le \mathbf{1}$ is a binary vector such that for the $k$th element $\boldsymbol{\delta}_{cd_k} = 1$ indicates charging and $\boldsymbol{\delta}_{cd_k} = 0$ indicates discharging. The scalar constants $p_{\text{bat}}^{gc,\max}, p_{\text{bat}}^{gd,\max}$ represent maximum green zone charging/discharging power rates, while $p_{\text{bat}}^{rc,\max}$ and $p_{\text{bat}}^{rd,\max}$ are maximum incremental red zone charging/discharging power rates.

The controller also decides whether the microgrid draws power from the outside grid (buying state), or power flows from the local microgrid to the outside grid (selling state). The following constraints impact the magnitude of battery charging/discharging power rates that relate to buying/selling state decisions:

$$\mathbf{P}_s^{d_b\,\max}(\mathbf{1} - \boldsymbol{\delta}_{bs2}) \le \mathbf{p}_s^{d_b} \le \mathbf{P}_s^{d_b\,\max}\mathbf{1}, \quad (6)$$

$$\mathbf{0} \le \mathbf{p}_s^{d_s} \le \left(p_{\text{bat}}^{gd,\max} + p_{\text{bat}}^{rd,\max}\right)(\mathbf{1} - \boldsymbol{\delta}_{bs2}) \quad (7)$$

$$\mathbf{P}_s^{c_s\,\max}\boldsymbol{\delta}_{bs1} \le \mathbf{p}_s^{c_s} \le \mathbf{P}_s^{c_s\,\max}\mathbf{1}, \quad (8)$$

$$\mathbf{0} \le \mathbf{p}_s^{c_b} \le (p_{\text{bat}}^{gc,\max} + p_{\text{bat}}^{rc,\max})\,\boldsymbol{\delta}_{bs1} \quad (9)$$

TABLE I
GRID FLOW DECISIONS—NET DEMAND KNOWN

| $\boldsymbol{\delta}_{cd_k}$ | $\boldsymbol{\delta}_{bs1_k}$ | $\boldsymbol{\delta}_{bs2_k}$ | $\mathbf{p}_{d_k} > 0$ | $\mathbf{p}_{d_k} < 0$ |
|---|---|---|---|---|
| 0 | 0 | 0 | sell* | sell |
| 0 | 0 | 1 | buy | sell$^+$ |
| 0 | 1 | 0 | sell* | *infeasible* |
| 0 | 1 | 1 | buy | *infeasible* |
| 1 | 0 | 0 | *infeasible* | sell |
| 1 | 0 | 1 | buy$^+$ | sell |
| 1 | 1 | 0 | *infeasible* | buy* |
| 1 | 1 | 1 | buy | buy* |

*may not be possible due to storage power limits
$^+$indicates storage power activity is zero

where $\mathbf{0} \le \boldsymbol{\delta}_{\text{bsi}} \le \mathbf{1}, i = 1, 2$ and

$$\mathbf{P}_{s_{k,k}}^{d_b\,\max} = \min\left(\max(0, \mathbf{p}_{d_k}), p_{\text{bat}}^{gd,\max} + p_{\text{bat}}^{rd,\max}\right) \quad (10)$$

$$\mathbf{P}_{s_{k,k}}^{c_s\,\max} = \min\left(\max(0, -\mathbf{p}_{d_k}), p_{\text{bat}}^{gc,\max} + p_{\text{bat}}^{rc,\max}\right) \quad (11)$$

for $k \in [1, N_h]$; note "$k, k$" points to a diagonal element. The binary vectors $\boldsymbol{\delta}_{bs1}$ and $\boldsymbol{\delta}_{bs2}$ are used to make buy/sell state decisions. The truth table in Table I indicates the different possible scenarios. The constraints in (7)–(9) are designed such that power rates $\mathbf{p}_s^{d_b}$ and $\mathbf{p}_s^{c_s}$ are utilized first for discharging and charging respectively; also note that their maximums, given in (10) and (11), depend on the net demand $\mathbf{p}_d$.

### *A. Battery Energy and Power Rate Change Constraints*

To ensure that at each time step in the horizon battery energy levels remain within certain bounds, given battery model (1), one can employ

$$E_{\text{bat}}^{\min} \le \eta_c \sum_{i=1}^{k} \mathbf{h}_i (\mathbf{p}_{\text{bat}_i}^{gc} + \mathbf{p}_{\text{bat}_i}^{rc}) - P_{\text{bat}}^{\text{loss}} \sum_{i=1}^{k} \mathbf{h}_i$$
$$-\eta_d^{-1} \sum_{i=1}^{k} \mathbf{h}_i (\mathbf{p}_{\text{bat}_i}^{gd} + \mathbf{p}_{\text{bat}_i}^{rd}) + E_{\text{bat}}^{o} \le E_{\text{bat}}^{\max}, k \in [1, N_h] \quad (12)$$

where $E_{\text{bat}}^{o}$ is the energy level at the start of the horizon, and $E_{\text{bat}}^{\min}$ and $E_{\text{bat}}^{\max}$ are lower and upper bounds, respectively.

The end of horizon battery energy level can be set via

$$\eta_c \mathbf{h}^T (\mathbf{p}_{\text{bat}}^{gc} + \mathbf{p}_{\text{bat}}^{rc}) - \eta_d^{-1} \mathbf{h}^T \left(\mathbf{p}_{\text{bat}}^{gd} + \mathbf{p}_{\text{bat}}^{rd}\right)$$
$$- P_{\text{bat}}^{\text{loss}} \mathbf{h}^T \mathbf{1} = E_{\text{bat}}^{\text{final}} - E_{\text{bat}}^{o} \quad (13)$$

where $E_{\text{bat}}^{\text{final}}$ is the desired end of horizon battery energy level. Without this constraint, the optimization would produce a charging/discharging profile over the prediction horizon that would drain all the stored energy. It is worthy to note that since a rolling horizon control approach is employed, any negative effects of omitting (13) can in many cases be negligibly small. Constraints related to battery signal smoothing and power rate change limits are given by

$$-\Delta p_{\text{bat}} \mathbf{h} \le -\mathbf{u}_{b_k} \le \mathbf{p}_{\text{bat}_k}^{gc} + \mathbf{p}_{\text{bat}_k}^{rc} - \mathbf{p}_{\text{bat}_k}^{gd} - \mathbf{p}_{\text{bat}_k}^{rd}$$
$$- \mathbf{p}_{\text{bat}_{k-1}}^{gc} - \mathbf{p}_{\text{bat}_{k-1}}^{rc} + \mathbf{p}_{\text{bat}_{k-1}}^{gd} + \mathbf{p}_{\text{bat}_{k-1}}^{rd} \le \mathbf{u}_{b_k} \le \Delta p_{\text{bat}} \mathbf{h} \quad (14)$$

for $k \in [1, N_h]$ and $\mathbf{u}_b \geq \mathbf{0}$. The term $\Delta p_{\text{bat}}$ represents the maximum allowed battery power rate change typically given in units of kW/h. Smoothing the battery power profile reduces transients that could otherwise be harmful to battery life.

### B. Battery Red-Zone Power Rate Constraints

The optimization can decide when to enable/disable battery red zone incremental power rates by using the following:

$$\mathbf{0} \leq \mathbf{p}_{\text{bat}}^{r\gamma} \leq p_{\text{bat}}^{r\gamma,max} \boldsymbol{\delta}_r \tag{15}$$

where $\gamma = c, d$ and the elements of binary vector $\mathbf{0} \leq \boldsymbol{\delta}_r \leq \mathbf{1}$ indicate when incremental red-zone power rates are active. To ensure green-zone power rates are first used the following constraints are needed:

$$p_{\text{bat}}^{gc,\max} \boldsymbol{\delta}_r - p_{\text{bat}}^{gc,\max}(\mathbf{1} - \boldsymbol{\delta}_{cd}) \leq \mathbf{p}_{\text{bat}}^{gc} \tag{16}$$

$$p_{\text{bat}}^{gd,\max} \boldsymbol{\delta}_r - p_{\text{bat}}^{gd,\max} \boldsymbol{\delta}_{cd} \leq \mathbf{p}_{\text{bat}}^{gd}. \tag{17}$$

It is assumed the red-zone power rates can be active for a limited amount of time and thus have a maximum on-time denoted by $T^{\text{maxon}}$. Moreover it is also assumed that a minimum cool down like time period is required before the red-zone power rates can be reactivated; this minimum off-time is denoted by $T^{\text{minoff}}$. The maximum on-time and minimum off-time constraints considering variable time steps in the horizon are formulated as

$$\sum_{k=j}^{j+T_j^{\text{maxon}}} \mathbf{h}_k \boldsymbol{\delta}_{r_k} \leq T^{\text{maxon}}, \forall j \in [j_{\min}, j_{\max}] \tag{18a}$$

$$j_{\min} = 2 - \min_{\mathbf{h}_1 \ell > T^{\text{maxon}}} \ell \in \mathbb{Z} \tag{18b}$$

$$j_{\max} = \max_{\sum_{k=\gamma}^{N_h} \mathbf{h}_k > T^{\text{maxon}}} \gamma \in \mathbb{Z} \tag{18c}$$

$$T_j^{\text{maxon}} = \min_{\sum_{k=j}^{j+\tau} \mathbf{h}_k > T^{\text{maxon}}} \tau \in \mathbb{Z} \tag{18d}$$

$$\boldsymbol{\delta}_{r_{j-k-1}} - \boldsymbol{\delta}_{r_{j-k}} \leq 1 - \boldsymbol{\delta}_{r_j}, \forall k \in [1, T_j^{\text{minoff}} - 1] \tag{19a}$$

$$\forall j \in \left\{ [1, N_h] \middle| \, T_j^{\text{minoff}} \geq 2 \right\} \tag{19b}$$

$$T_j^{\text{minoff}} = \min_{\sum_{k=j-\tau}^{j-1} \mathbf{h}_k \geq T^{\text{minoff}}} \tau \in \mathbb{Z}, \tau \geq 1 \tag{19c}$$

where the first element $\mathbf{h}_k = \mathbf{h}_1$ is used when $k \leq 0$. Note that a history of previous red-zone activity is needed, the time length of which is dictated by $T^{\text{maxon}}$ and $T^{\text{minoff}}$. These past binary values are treated as constants in the inequality constraints. The maximum on-time constraints are given in (18). These constraints function by scanning rolling windows of time length just greater than $T^{\text{maxon}}$. In (19) the minimum off-time constraints are shown, which operate by scanning sufficiently back in time such that the last time red-zone activity was disabled does not occur within the last $T^{\text{minoff}}$ hours. The terms in (18b)–(18d) and (19c) are used to find the correct range of integer indices in the variable time step horizon. They can be precomputed by using only $\mathbf{h}, T^{\text{maxon}}$ and $T^{\text{minoff}}$. Note that in (19b), only indices that satisfy $T_j^{\text{minoff}} \leq 2$ are included.

### C. Grid Signal Shaping Constraints

The A-EMS controller can shape the power profile of the microgrid at the point of common coupling with the grid. This is a desirable feature since it would help generate a well-behaved and more predictable load response from the grid perspective. To enable peak shaving and reduction over some baseline, the following inequality constraint is employed:

$$\mathbf{p}_{\text{bat}}^{gc} + \mathbf{p}_{\text{bat}}^{rc} - \mathbf{p}_{\text{bat}}^{gd} - \mathbf{p}_{\text{bat}}^{rd} + \mathbf{p}_d \leq p_g^{\text{base}} \mathbf{1} + p_g^{ob} \mathbf{1} \tag{20}$$

where $p_g^{ob} \geq 0$. Grid signal flattening or squeezing requires the inequalities

$$p_g^{\min} \mathbf{1} \leq \mathbf{p}_s^{c_s} + \mathbf{p}_s^{c_b} - \mathbf{p}_s^{d_b} - \mathbf{p}_s^{d_s} + \mathbf{p}_d \leq p_g^{\max} \mathbf{1} \tag{21}$$

where $p_g^{\min}$ and $p_g^{\max}$ are scalar optimization variables corresponding to minimum and maximum grid power rates. Grid signal smoothing of successive grid power rate changes is achieved by

$$\begin{aligned} -\mathbf{u}_{g_k} \leq \mathbf{p}_{s_k}^{c_s} + \mathbf{p}_{s_k}^{c_b} - \mathbf{p}_{s_k}^{d_b} - \mathbf{p}_{s_k}^{d_s} + \mathbf{p}_{d_k} - \mathbf{p}_{d_{k-1}} \\ - \mathbf{p}_{s_{k-1}}^{c_s} - \mathbf{p}_{s_{k-1}}^{c_b} + \mathbf{p}_{s_{k-1}}^{d_b} + \mathbf{p}_{s_{k-1}}^{d_s} \leq \mathbf{u}_{g_k} \end{aligned} \tag{22}$$

for $k \in [1, N_h]$ and $\mathbf{u}_g \geq \mathbf{0}$. When $k = 1$, past grid power activity and net demand from the previous time-step or iteration of the rolling horizon controller are needed.

### D. Decision Variables

The non-robust MILP optimization seeks to find optimal values for the following vectors/variables:

$$\begin{aligned} &\mathbf{p}_s^{c_s}, \mathbf{p}_s^{c_b}, \mathbf{p}_s^{d_b}, \mathbf{p}_s^{d_s}, \mathbf{p}_{\text{bat}}^{gc}, \mathbf{p}_{\text{bat}}^{rc}, \mathbf{p}_{\text{bat}}^{gd}, \mathbf{p}_{\text{bat}}^{rd}, \mathbf{u}_g, \mathbf{u}_b \in \Re^{N_h} \\ &p_g^{ob}, p_g^{\max}, p_g^{\min} \in \Re \\ &\boldsymbol{\delta}_{bs1}, \boldsymbol{\delta}_{bs2}, \boldsymbol{\delta}_{cd}, \boldsymbol{\delta}_r \in \mathbb{Z}^{N_h} \end{aligned}$$

to linear constraints (3)–(22).

## III. Robust Optimization Approach

This section presents a robust MILP counterpart optimization formulation that is robust to a predicted and uncertain net demand vector. Uncertainties are assumed to appear in the net demand prediction vector $\mathbf{p}_d$. This vector is assumed to have bounded errors and satisfies

$$\bar{\mathbf{p}}_d - \Delta \bar{\mathbf{p}}_d = \mathbf{p}_d^{\min} \leq \mathbf{p}_d \leq \mathbf{p}_d^{\max} = \bar{\mathbf{p}}_d + \Delta \bar{\mathbf{p}}_d \tag{23}$$

where vector $\bar{\mathbf{p}}_d$ denotes an estimate of net demand with bounded error vector $\Delta \bar{\mathbf{p}}_d$.

In [21], a method is presented to convert an inequality constraint with uncertainties into a robust counterpart form while retaining linearity [21]. The nonrobust optimization was able to make hard decisions regarding buy/selling to the grid since it assumed the net demand vector was known. The presence of bounded uncertainty in the predicted net demand leads to an additional *uncertain* buying/selling state as depicted in Fig. 5 for different cases of net demand. The magnitude of charging/discharge battery storage can lead to three possible states: buying/

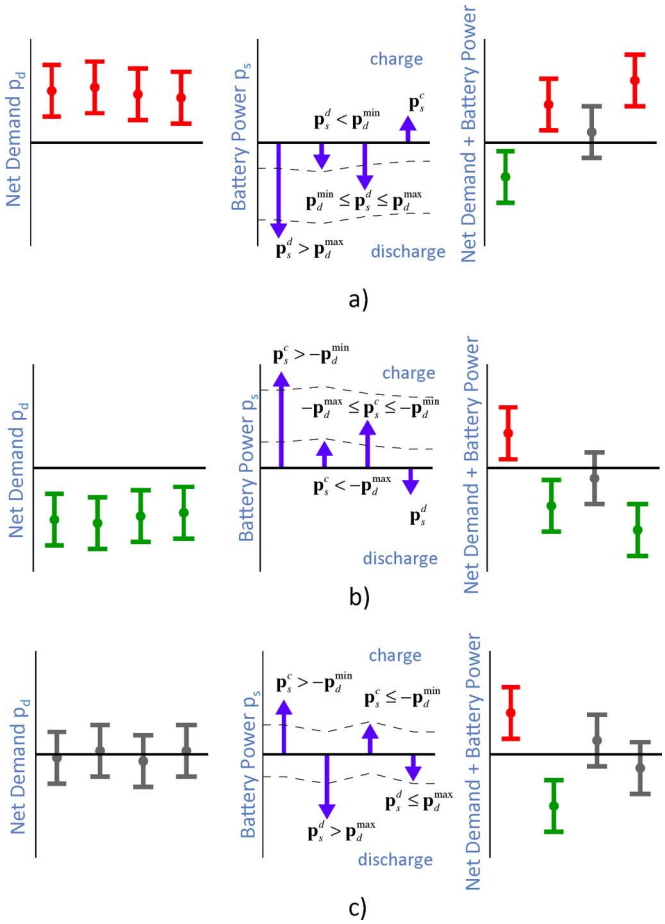


Fig. 5. Buy/uncertain/sell states for different cases, the charge/discharge power vectors can be split into three components: $\mathbf{p}_s^c = \mathbf{p}_s^{c_s} + \mathbf{p}_s^{c_u} + \mathbf{p}_s^{c_b}, \mathbf{p}_s^d = \mathbf{p}_s^{d_b} + \mathbf{p}_s^{c_u} + \mathbf{p}_s^{d_s}$. (a) Net demand positive $\mathbf{p}_s^{c_s} = \mathbf{p}_s^{c_u} = \mathbf{0}$. (b) Net demand negative $\mathbf{p}_s^{d_b} = \mathbf{p}_s^{d_u} = \mathbf{0}$. (c) Net demand uncertain $\mathbf{p}_s^{c_s} = \mathbf{p}_s^{d_b} = \mathbf{0}$.

uncertain/selling. As a result the power balance equality constraints (3) are replaced with

$$\mathbf{p}_s^{c_s} + \mathbf{p}_s^{c_u} + \mathbf{p}_s^{c_b} = \mathbf{p}_{\text{bat}}^{gc} + \mathbf{p}_{\text{bat}}^{rc} \tag{24}$$

$$\mathbf{p}_s^{d_b} + \mathbf{p}_s^{d_u} + \mathbf{p}_s^{d_s} = \mathbf{p}_{\text{bat}}^{gd} + \mathbf{p}_{\text{bat}}^{rd} \tag{25}$$

where the additional terms $\mathbf{p}_s^{c_u}$ and $\mathbf{p}_s^{d_u}$ represent the portion of storage power corresponding to the uncertain state for charging and discharging, respectively. For example, the first and third blue down arrows in Fig. 5(a) and the blue down arrows in Fig. 5(c) all have a nonzero $\mathbf{p}_s^{d_u}$. In Fig. 5(a) and (c), the first and third blue arrows all have nonzero $\mathbf{p}_s^{c_u}$. With the addition of these two extra power vectors, (2a) must be modified to

$$\begin{aligned}\min \big( \cancel{\mathbf{c}_{bs}^T \mathbf{p}_d} + \mathbf{c}_{\text{sell}}^T \mathbf{p}_s^{c_s} + \mathbf{c}_{bs,c}^T \mathbf{p}_s^{c_u} + \mathbf{c}_{\text{buy}}^T \mathbf{p}_s^{c_b} \\ - \mathbf{c}_{\text{buy}}^T \mathbf{p}_s^{d_b} - \mathbf{c}_{bs,d}^T \mathbf{p}_s^{d_u} - \mathbf{c}_{\text{sell}}^T \mathbf{p}_s^{d_s}\end{aligned} \tag{26}$$

where $\mathbf{c}_{bs}, \mathbf{c}_{bs,c}$ and $\mathbf{c}_{bs,d}$ are uncertain cost coefficient vectors that depend on $\mathbf{p}_d$. It can be proven that these vectors take values in the range $[\min(\mathbf{c}_{\text{buy}}, \mathbf{c}_{\text{sell}}), \max(\mathbf{c}_{\text{buy}}, \mathbf{c}_{\text{sell}})]$. Although the term $\mathbf{c}_{bs}^T \mathbf{p}_d$ is uncertain, it is not affected by the optimization decision variables, and therefore it is eliminated from the cost function. The other cost terms in (2b) and (2c) remain unchanged.

The two remaining uncertain cost vectors have estimates and bounded errors given by

$$\bar{\mathbf{c}}_{bs,\gamma} = 0.5\left(\mathbf{c}_{\text{buy}} + \mathbf{c}_{\text{sell}}\right), \Delta\bar{\mathbf{c}}_{bs,\gamma} = 0.5|\mathbf{c}_{\text{buy}} - \mathbf{c}_{\text{sell}}| \tag{27}$$

where $\gamma = c$ or $d$.

Using (2b), (2c), and (26) with estimates/bounds in (27) and robust counterpart formation of the constraints, the minimum robust worst case cost of (2) becomes

$$\min\ t \quad \text{subject to} \tag{28}$$

$$\mathbf{c}_{\text{sell}}^T \mathbf{p}_s^{c_s} + 0.5(\mathbf{c}_{\text{buy}} + \mathbf{c}_{\text{sell}})^T \mathbf{p}_s^{c_u} + \mathbf{c}_{\text{buy}}^T \mathbf{p}_s^{c_b} \tag{29a}$$

$$- \mathbf{c}_{\text{buy}}^T \mathbf{p}_s^{d_b} - 0.5(\mathbf{c}_{\text{buy}} + \mathbf{c}_{\text{sell}})^T \mathbf{p}_s^{d_u} - \mathbf{c}_{\text{sell}}^T \mathbf{p}_s^{d_s} \tag{29b}$$

$$+ \mathbf{c}_{\text{batg}}^T \left(\mathbf{p}_{\text{bat}}^{gc} + \mathbf{p}_{\text{bat}}^{gd}\right) + \mathbf{c}_{\text{batr}}^T \left(\mathbf{p}_{\text{bat}}^{rc} + \mathbf{p}_{\text{bat}}^{rd}\right) + \mathbf{c}_{smb}^T \mathbf{u}_b \tag{29c}$$

$$+ \mathbf{c}_{smg}^T \mathbf{u}_g + c_{\text{peak}} p_g^{ob} + c_{\text{flat}} \left(p_g^{\max} - p_g^{\min}\right) \tag{29d}$$

$$+ \Gamma z_c + \Gamma z_d + \mathbf{1}^T \mathbf{w}_c + \mathbf{1}^T \mathbf{w}_d \le t \tag{29e}$$

where $t, z_c, z_d, \mathbf{w}_c$ and $\mathbf{w}_d$ are additional auxiliary variables needed for the robust worst case optimization [21]. The following extra robust counterpart constraints are also needed

$$0.5|\mathbf{c}_{buy_j} - \mathbf{c}_{sell_j}|\mathbf{p}_{s_j}^{\gamma_u} \le z_\gamma + \mathbf{w}_{\gamma_j}, j \in [1, N_h], \gamma = c, d \tag{30}$$

$$0 \le z_c, 0 \le z_d, \mathbf{0} \le \mathbf{w}_c, \mathbf{0} \le \mathbf{w}_d \tag{31}$$

The robust optimization makes decisions as to whether charge or discharge the battery, therefore it also uses constraints (4) and (5). However, grid flow condition now becomes either buying state, uncertain state, or selling state. To enable this in addition to (7)–(9), the following extra buy/uncertain/sell state decision constraints are required

$$\mathbf{P}_s^{d_b\,\max}(\mathbf{1} - \boldsymbol{\delta}_{bs1}) \le \mathbf{p}_s^{d_b} \tag{32}$$

$$\mathbf{P}_s^{d_u\,\max}(\mathbf{1} - \boldsymbol{\delta}_{bs2}) \le \mathbf{p}_s^{d_u} \le \mathbf{P}_s^{d_u\,\max}(\mathbf{1} - \boldsymbol{\delta}_{bs1}) \tag{33}$$

$$\mathbf{P}_s^{c_s\,\max}\boldsymbol{\delta}_{bs2} \le \mathbf{p}_s^{c_s} \tag{34}$$

$$\mathbf{P}_s^{c_u\,\max}\boldsymbol{\delta}_{bs1} \le \mathbf{p}_s^{c_u} \le \mathbf{P}_s^{c_u\,\max}\boldsymbol{\delta}_{bs2} \tag{35}$$

where

$$\begin{aligned}\mathbf{P}_{s_{k,k}}^{d_u\,\max} = \min \Big(&p_{\text{bat}}^{gd,\max} + p_{\text{bat}}^{rd,\max}, \\ &\max\left(0, \bar{\mathbf{p}}_{d_k} + \Delta\bar{\mathbf{p}}_{d_k}\right) - \max\left(0, \bar{\mathbf{p}}_{d_k} - \Delta\bar{\mathbf{p}}_{d_k}\right)\Big)\end{aligned} \tag{36}$$

$$\begin{aligned}\mathbf{P}_{s_{k,k}}^{c_u\,\max} = \min \Big(&p_{\text{bat}}^{gc,\max} + p_{\text{bat}}^{rc,\max}, \\ &\min\left(0, \bar{\mathbf{p}}_{d_k} + \Delta\bar{\mathbf{p}}_{d_k}\right) - \min\left(0, \bar{\mathbf{p}}_{d_k} - \Delta\bar{\mathbf{p}}_{d_k}\right)\Big)\end{aligned} \tag{37}$$

and (10) and (11) are replaced with

$$\begin{aligned}\mathbf{P}_{s_{k,k}}^{d_b\,\max} &= \min\left(\max\left(0, \bar{\mathbf{p}}_{d_k} - \Delta\bar{\mathbf{p}}_{d_k}\right), p_{\text{bat}}^{gd,\max} + p_{\text{bat}}^{rd,\max}\right) \\ \mathbf{P}_{s_{k,k}}^{c_s\,\max} &= \min\left(\max\left(0, -\bar{\mathbf{p}}_{d_k} - \Delta\bar{\mathbf{p}}_{d_k}\right), p_{\text{bat}}^{gc,\max} + p_{\text{bat}}^{rc,\max}\right)\end{aligned} \tag{38}$$

for $k \in [1, N_h]$; note that "$k, k$" points to a diagonal element. The truth table for the different grid-flow states under different net demand conditions is given in Table II.

TABLE II
GRID FLOW DECISIONS—NET DEMAND UNKNOWN

| $\boldsymbol{\delta}_{cd_k}$ | $\boldsymbol{\delta}_{bs1_k}$ | $\boldsymbol{\delta}_{bs2_k}$ | $0<\mathbf{p}_{d_k}^{\min}<\mathbf{p}_{d_k}^{\max}$ | $\mathbf{p}_{d_k}^{\min}<\mathbf{p}_{d_k}^{\max}<0$ | $\mathbf{p}_{d_k}^{\min}<0<\mathbf{p}_{d_k}^{\max}$ |
|---|---|---|---|---|---|
| 0 | 0 | 0 | sell* | sell | sell* |
| 0 | 0 | 1 | uncertain* | *infeasible* | uncertain |
| 0 | 1 | 0 | *infeasible* | *infeasible* | *infeasible* |
| 0 | 1 | 1 | buy | *infeasible* | *infeasible* |
| 1 | 0 | 0 | *infeasible* | sell | *infeasible* |
| 1 | 0 | 1 | *infeasible* | uncertain* | uncertain |
| 1 | 1 | 0 | *infeasible* | *infeasible* | *infeasible* |
| 1 | 1 | 1 | buy | buy* | buy* |

*may not be possible due to storage power limits

The battery energy, power rate, and red zone constraints in (12)–(19) are unchanged. The peak demand over some baseline constraint (20) becomes

$$\mathbf{p}_{\text{bat}}^{gc}+\mathbf{p}_{\text{bat}}^{rc}-\mathbf{p}_{\text{bat}}^{gd}-\mathbf{p}_{\text{bat}}^{rd}+\bar{\mathbf{p}}_d+\Delta\bar{\mathbf{p}}_d\leq p_g^{\text{base}}\mathbf{1}+p_g^{ob}\mathbf{1} \tag{39}$$

where $p_g^{ob}\geq 0$. The grid signal flattening constraint (21) is replaced with robust constraints

$$\mathbf{p}_s^{c_s}+\mathbf{p}_s^{c_u}+\mathbf{p}_s^{c_b}-\mathbf{p}_s^{d_b}-\mathbf{p}_s^{d_u}-\mathbf{p}_s^{d_s}+\bar{\mathbf{p}}_d+\Delta\bar{\mathbf{p}}_d\leq p_g^{\max}\mathbf{1} \tag{40}$$

$$p_g^{\min}\mathbf{1}\leq\mathbf{p}_s^{c_s}+\mathbf{p}_s^{c_u}+\mathbf{p}_s^{c_b}-\mathbf{p}_s^{d_b}-\mathbf{p}_s^{d_u}-\mathbf{p}_s^{d_s}+\bar{\mathbf{p}}_d-\Delta\bar{\mathbf{p}}_d. \tag{41}$$

The grid signal smoothing constraint (22) is replaced with robust counterparts

$$\begin{aligned}&-\mathbf{u}_{g_k}+\Delta\bar{\mathbf{p}}_{d_{k-1}}+\Delta\bar{\mathbf{p}}_{d_k}\\&\quad\leq\mathbf{p}_{s_k}^{c_s}+\mathbf{p}_{s_k}^{c_u}+\mathbf{p}_{s_k}^{c_b}-\mathbf{p}_{s_k}^{d_b}-\mathbf{p}_{s_k}^{d_u}-\mathbf{p}_{s_k}^{d_s}+\bar{\mathbf{p}}_{d_k}\\&\qquad-\mathbf{p}_{s_{k-1}}^{c_s}-\mathbf{p}_{s_{k-1}}^{c_u}-\mathbf{p}_{s_{k-1}}^{c_b}+\mathbf{p}_{s_{k-1}}^{d_b}+\mathbf{p}_{s_{k-1}}^{d_u}-\bar{\mathbf{p}}_{d_{k-1}}\\&\quad\leq\mathbf{u}_{g_k}-\Delta\bar{\mathbf{p}}_{d_{k-1}}-\Delta\bar{\mathbf{p}}_{d_k}\end{aligned} \tag{42}$$

for $k\in[1,N_h]$ and $\mathbf{u}_g\geq\mathbf{0}$.

*Computation Cost:* The robust MILP formulation has $18N_h+6$ variables compared to $14N_h+3$ for the nonrobust formulation. The additional variables include: $t,z_c,z_d\in\Re$ and $\mathbf{w}_c,\mathbf{w}_d,\mathbf{p}_s^{d_u},\mathbf{p}_s^{c_u}\in\Re^{N_h}$. It is noted here that none of these additional variables are binary; therefore, the additional computational cost follows polynomial time computational complexity of solving linear programs. Computational time complexity for linear programs can be bounded to $O(n^{3.5})$ time, where $n$ is the number of variables [22]. Choosing $N_h=22$, the robust MILP would increase computational time by at most a factor of 2.4.

## IV. SIMULATION RESULTS

Simulations are performed under a variety of conditions to demonstrate the different features of the robust MILP-based rolling horizon controller. Matlab is used with the IBM ILOG CPLEX MILP optimization solver. Real electricity usage data for a commercial/residential setting (peak usage less than 50 kW), an industrial setting (peak usage over 50 kW), and a solar power generation station (up to 30 kW capable), provided by Burlington Hydro Inc. (Burlington, ON, Canada) has been used in the simulations. In each case, uniform random noise of up to the square root of the usage data is added to evaluate robustness of the controller to uncertainty in load and generation.

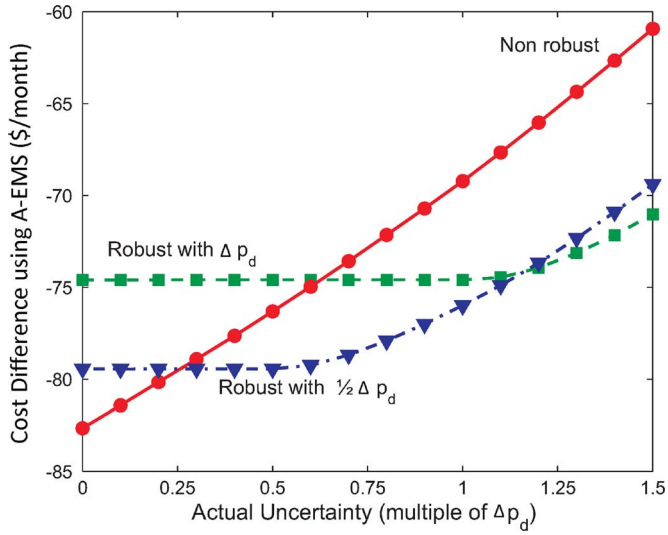


Fig. 6. Comparison of the nonrobust and robust controllers when time of use electricity pricing is used and the selling price is set to zero. Note that for the robust controllers, $(1)/(2)\Delta\mathbf{p}_d$ and $\Delta\mathbf{p}_d$ denote the estimated uncertainty range used in the optimization. The actual uncertainty in the demand data is indicated as a multiple of $\Delta\mathbf{p}_d$ along the horizontal axis.

### A. Effect of Robustness on Savings With Time-of-Use Pricing

A commercial/residential setting is considered where winter time of use electricity pricing is used, i.e., 6.2 ¢/kWh 7 pm–7 am, 9.2 ¢/kWh 11 am–5 pm, 10.8 ¢/kWh 7 am–11 am and 5 pm–7 pm [23]. All other costs are assumed zero. The battery characteristics are $E_{\text{bat}}^{\min}=0$ kWh, $E_{\text{bat}}^{\max}=50$ kWh, $p_{\text{bat}}^{gc,\max}=p_{\text{bat}}^{gd,\max}=p_{\text{bat}}^{rc,\max}=p_{\text{bat}}^{rd,\max}=10$ kW, $T^{\text{maxon}}=T^{\text{minoff}}=2$ h, $P_{\text{bat}}^{\text{loss}}=0$ kW, $\eta_c=0.95$, and $\eta_d=0.9$. The time horizon used was 96 $h$ with variable time-step vector $\mathbf{h}=[0.5\ 0.5\ 0.5\ 0.5\ 1\ 1\ 2\ 2\ 2\ 2\ 3\ 3\ 3\ 3\ 6\ 6\ 6\ 6\ 12\ 12\ 12\ 12]^T$; therefore, $N_h=22$ and the rolling horizon controller runs every half hour. The time of day, time of use rates and vector $\mathbf{h}$ specify cost vector $\mathbf{c}_{\text{buy}}$, for example at midnight $\mathbf{c}_{\text{buy}}=[3.1\ 3.1\ 3.1\ 3.1\ 6.2\ 6.2\ 12.4\ 17\ 21.6\ 20\ 27.6\ 29.2\ 23.2\ 18.6\ 37.2\ 58.6\ 56.8\ 41.8\ 95.8\ 98.6\ 95.8\ 98.6]^T$. The end of horizon battery energy level was chosen as $E_{\text{bat}}^{\text{final}}=E_{\text{bat}}^{o}$. One winter month is simulated with different magnitudes of actual uncertainty in the demand and with three different control cases: 1) a non-robust controller 2) a robust controller with $(1/2)\Delta\mathbf{p}_d$ estimated uncertainty, and 3) a robust controller with $\Delta\mathbf{p}_d$ estimated uncertainty. Here $\Delta\mathbf{p}_d$ is twice the square root of the actual demand. The savings results are plotted in Fig. 6. Since there is no revenue generated from selling electricity back to the grid ($\mathbf{c}_{\text{sell}}=\mathbf{0}$), the net demand prediction error degrades savings by excessively discharging the battery such that electricity is undesirably sent back to the grid. The robust controller tends to avoid this effect and as a result is less sensitive to uncertainty. It is worth noting that, as expected, the nonrobust controller outperforms its robust counterparts when the net predictions are accurate, i.e., the actual uncertainty is zero, but this quickly reverses as the

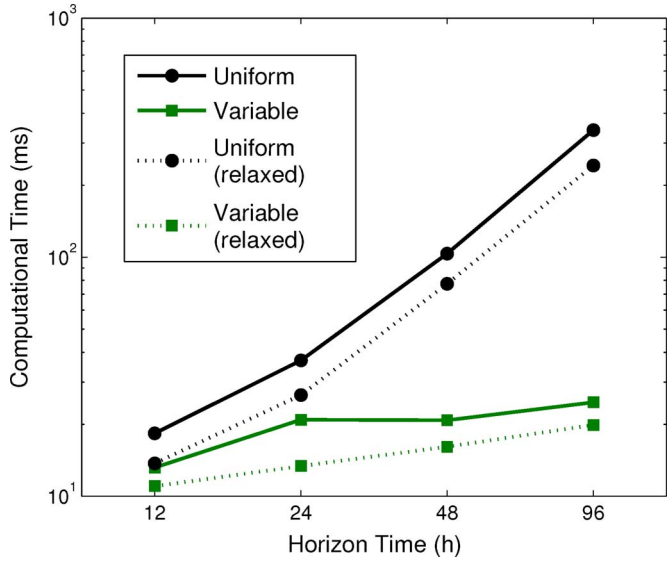


Fig. 7. Average robust MILP optimization computation time for different time step vectors and horizons using an Intel i5 2.5 GHz CPU with 4 GB ram runing Mac OS X. Note the y-axis is log scaled. The performance/cost objective value in each case are within 1% of each other.

errors in predictions increase. The performance of the robust controllers is insensitive to the actual uncertainty, as long as it falls within their expected range. Moreover, their performance degrade at a slower rate compared to the nonrobust controller, even as the actual uncertainty exceeds the expected range used in the optimization. Finally, it is noted that the computational time of solving the robust MILP was on average 24% longer than solving the non-robust MILP.

### *B. Effect of Uniform/Variable Time-Steps and Relaxation*

The same setting used in the previous subsection is also considered here; however, the time-step step vector $\mathbf{h}$ and time horizon are adjusted. Constraint relaxation is also examined by relaxing the binary constraints on all but the first time-step in the rolling horizon window. For uniform time steps the elements of $\mathbf{h}$ are all ones, e.g., for 96 h time horizon $\mathbf{h} = \mathrm{ones}(96, 1)$. For variable time step horizons all or a truncated portion of vector $[1\ 1\ 1\ 1\ 2\ 2\ 2\ 2\ 3\ 3\ 3\ 3\ 6\ 6\ 6\ 6\ 12\ 12\ 12\ 12]^T$ is used, e.g., for a 12-h time horizon $\mathbf{h} = [1\ 1\ 1\ 1\ 2\ 2\ 2\ 2]^T$. The average computation time of 720 iterations (one month) of the rolling horizon controller is shown in Fig. 7. It is noted that the ($ per month) savings for all the cases in Fig. 7 were nearly the same and within 1% of each other. It is clear that the use of variable time steps can greatly reduce computational costs by reducing the size of the optimization problem needed to be solved at each iteration of the rolling horizon controller. Relaxing binary constraints also to a lesser effect improves computation speed. It has the additional advantage of simplifying the optimization algorithm to solving a small number of linear programs.

### *C. Grid Signal and Battery Signal Shaping Features*

Here the power signal shaping features of the proposed rolling horizon controller are highlighted by adjusting the cost parameters/vectors and illustrating the effect of different grid signal and battery signal objectives. The same commercial/residential setting as in the previous simulations is used here; however, the battery characteristics are $E_{\mathrm{bat}}^{\min} = 0$ kWh, $E_{\mathrm{bat}}^{\max} = 15$ kWh, $p_{\mathrm{bat}}^{gc,\max} = p_{\mathrm{bat}}^{gd,\max} = p_{\mathrm{bat}}^{rc,\max} = p_{\mathrm{bat}}^{rd,\max} = 3$ kW, $T^{\mathrm{maxon}} = 0.5$ h, $T^{\mathrm{minoff}} = 2$ h, $P_{\mathrm{bat}}^{\mathrm{loss}} = 0$ kW, and $\eta_c = \eta_d = 1$. The buying/selling usage prices are set to zero, i.e., $\mathbf{c}_{\mathrm{buy}} = \mathbf{c}_{\mathrm{sell}} = \mathbf{0}$. The horizon vector is set as $h = [0.5\ 0.5\ 0.5\ 0.5\ 0.5\ 0.5\ 1\ 1\ 1\ 2\ 2\ 2\ 3\ 3\ 3\ 3]^T$.

Different grid signal shaping features are highlighted by setting the cost terms are follows: 1) peak reduction only $c_{\mathrm{peak}} = 1$ other costs zero, 2) flattening objective only $c_{\mathrm{flat}} = 1$ other costs zero, and 3) smoothing objective only $\mathbf{c}_{smg} = \mathbf{h}$ other costs zero. These different features are shown in Fig. 8 for a 24-hour time plot.

In Fig. 8(b) the running baseline term is initially set to $p_g^{\mathrm{base}} = 0$ and is increased only when necessary. These increases occur up to the 10-h mark, after which the rolling horizon controller is able to keep peak usage below that threshold. The grid signal flattening objective feature shown in Fig. 8(c) shows the desired squeezing effect of the net demand profile; it operates by considering both the upper and lower bounds of net demand prediction. The grid signal smoothing feature is shown in Fig. 8(d) where successive differences are minimized.

Battery signal shaping sub-objectives are then added to highlight their effect for the case of grid signal flattening. With no battery signal sub objectives, the battery power profile corresponding to Fig. 8(c) is shown in Fig. 9(a). It is worthy to note the battery red zone incremental rate constraints are enforced by observing these rates are only active for at most half an hour with minimum off-time between these rates of 2 h in all cases in Fig. 9. A battery usage sub-objective of $\mathbf{c}_{\mathrm{batg}} = \mathbf{c}_{\mathrm{batr}} = 0.001\mathbf{h}$ is added and its effect is depicted in Fig. 9(b). The battery usage cost effectively minimized the magnitude of battery charging/discharging. Next the battery usage cost is reset back to zero and replaced with a battery signal smoothing sub-objective with cost of $\mathbf{c}_{smb} = 0.001\mathbf{h}$. The resulting battery usage profile is shown in 9(c) and is comparatively smoother than those in Fig. 9(a) and (b). Finally both battery usage and smoothing sub-objectives of $\mathbf{c}_{\mathrm{batg}} = \mathbf{c}_{\mathrm{batr}} = 0.01\mathbf{h}$ and $\mathbf{c}_{smb} = 0.001\mathbf{h}$ are applied and their effect is shown in Fig. 9(d). It is noted that the addition of battery signal sub-objectives in each case yields nearly identical grid profiles to Fig. 8(c) with the same grid profile peak-to-peak values.

### *D. Demand and Time-of-Use Charges*

This case considers an industrial setting subject to both peak demand costs of $6 per kW and time-of-use electricity buying prices; summer time-of-use rates used are 6.2 ¢/kWh 7 pm–7 am, 10.8 ¢/kWh 11 am–5 pm, 9.2 ¢/kWh 7 am–11 am and 5 pm–7 pm [23]. Other costs terms are set to zero. The variable time step vector was set to $\mathbf{h} = [1\ 1\ 1\ 1\ 2\ 2\ 2\ 2\ 3\ 3\ 3\ 3]^T$. Battery red-zone rates were not employed and the battery characteristics are $E_{\mathrm{bat}}^{\min} = 0$ kWh, $E_{\mathrm{bat}}^{\max} = 200$ kWh, $p_{\mathrm{bat}}^{gc,\max} = p_{\mathrm{bat}}^{gd,\max} = 50$ kW, $P_{\mathrm{bat}}^{\mathrm{loss}} = 0$ kW, and $\eta_c = \eta_d = 1$. Three control methods are considered: an ideal case with no uncertainty and the nonrobust controller, uncertainty with the nonrobust controller, and

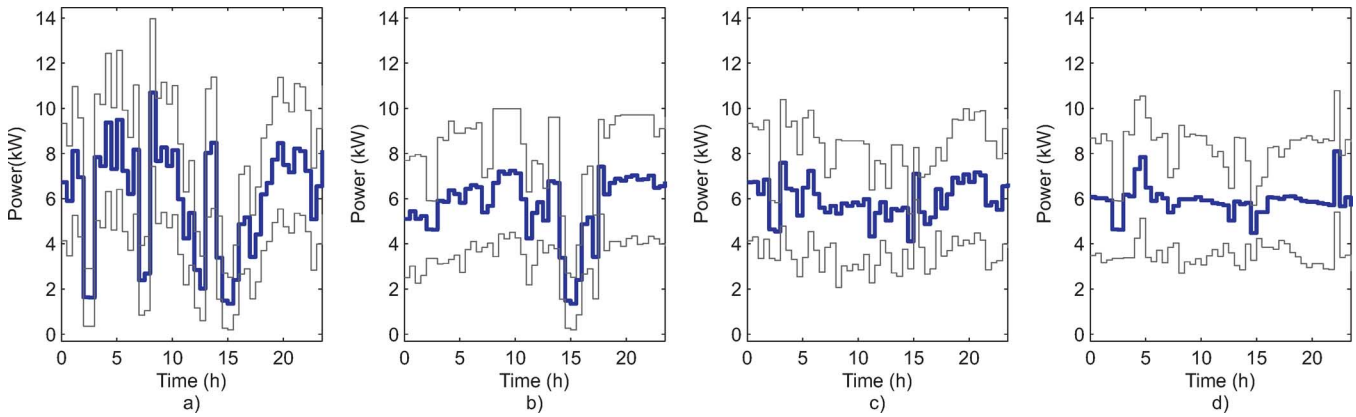


Fig. 8. Different robust grid signal shaping objectives. (a) Net demand profile; grid profile with no A-EMS. (b) Grid power profile with only peak demand reduction. (c) Grid power profile with only flattening objective. (d) Grid power profile with only smoothing objective. Note the thin black lines indicate upper and lower bounds.

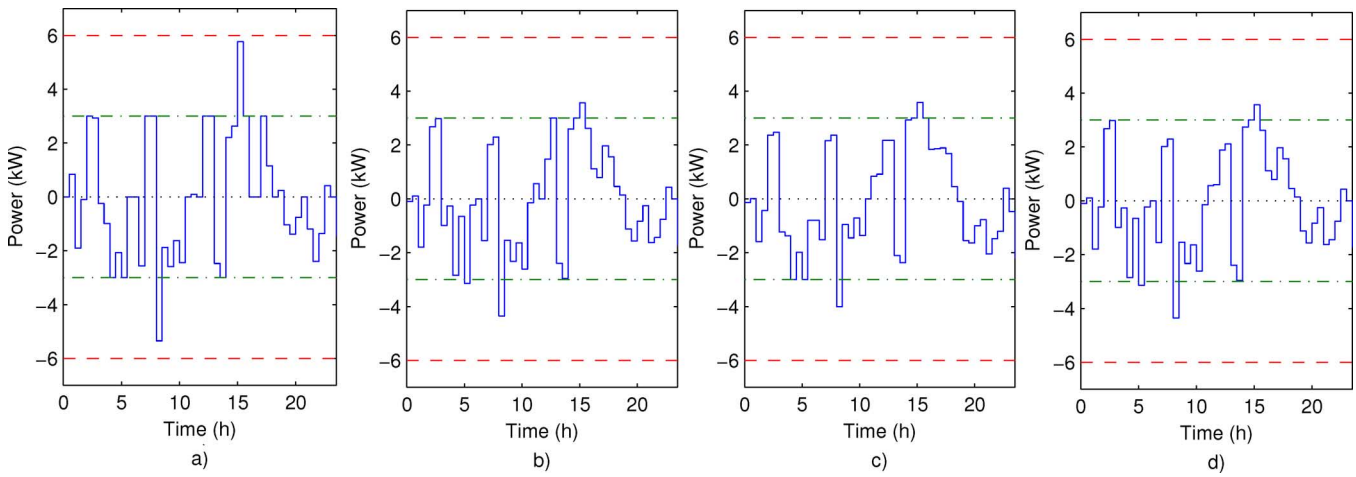


Fig. 9. Battery profile with grid flattening objective. (a) No sub-objectives. (b) Battery usage sub-objective. (c) Battery signal smoothing sub-objective. (d) Battery usage and smoothing sub-objectives. Note the dot-dashed (green) line indicate green zone power rate limits, and the dashed lines indicate maximum, in red zone, battery power limits.

TABLE III
SAVINGS FOR DIFFERENT CONTROL AND $E_{\text{bat}}^{\text{final}}$ CONDITIONS

| | $E_{bat}^{final} = E_{bat}^{o}$ | $E_{bat}^{final} = 0$ | Optimized |
|---|---|---|---|
| No uncertainty | 561 ± 2.6 | 564 ± 1.3 | 564 ± 1.5 |
| Non-robust | 392 ± 17.1 | 390 ± 18.8 | 390 ± 18.2 |
| Robust | 533 ± 14.5 | 523 ± 14.5 | 523 ± 14.5 |

uncertainty with the robust controller. Three different end of horizon battery level conditions are also tested. The results are shown in Table III where each condition represents the average of 10 monthly profiles; each profile represents a summer month with different random perturbations added to the same month. The optimized method uses the approach described in Section II where the additional variable $E_{\text{bat}}^{*} = E_{\text{bat}}^{o} = E_{\text{bat}}^{\text{final}}$ is added to the first optimization routine; this approach effectively doubles the computational cost. It is observed the robust controller improves performance in the presence of prediction error. The differences between $E_{\text{bat}}^{\text{final}}$ conditions appear negligible. This highlights a well-known property of rolling horizon control, that it has an advantage of being able to perpetually avoid undesirable control actions. However, this can also be a disadvantage since perpetually avoiding beneficial actions, such as profit taking, is also possible.

### E. Grid Signal Flattening With Solar Power Production

In this scenario, the A-EMS takes advantage of local battery storage and solar energy to flatten the microgrid power demand profile. The microgrid load is the same as in Fig. 8. The battery characteristics are $E_{\text{bat}}^{\min} = 0$ kWh, $E_{\text{bat}}^{\max} = 0 - 200$ kWh, $p_{\text{bat}}^{gc,\max} = p_{\text{bat}}^{gd,\max} = p_{\text{bat}}^{rc,\max} = p_{\text{bat}}^{rd,\max} = 10$ kW, $T^{\text{maxon}} = T^{\text{minoff}} = 2$ h, $P_{\text{bat}}^{\text{loss}} = 0$ kW, $\eta_c = 0.95$, and $\eta_d = 0.9$. A time horizon of 96 $h$ with variable time step vector $\mathbf{h} = [0.5\ 0.5\ 0.5\ 0.5\ 1\ 1\ 2\ 2\ 2\ 2\ 3\ 3\ 3\ 3\ 6\ 6\ 6\ 6\ 12\ 12\ 12\ 12]^T$ is employed. The grid flattening cost is $c_{\text{flat}} = 1$ with sub-objectives of grid and battery smoothing $\mathbf{c}_{smg} = \mathbf{c}_{\text{batg}} = \mathbf{c}_{\text{batr}} = 0.001\mathbf{h}$. All other costs are set to zero. Simulated profiles for seven days assuming a battery size of 100 kWh is shown in Fig. 10. Note that due to solar production, the net demand can be both positive and negative. The effect of battery size is explored in Fig. 11, which highlights diminishing returns as a function of the battery capacity for sufficiently large battery sizes. Increasing battery power size alone can no longer shape the grid signal toward a desired non-fluctuating power source.

## V. CONCLUSION

MILP-based rolling horizon controllers were proposed for electric only microgrids employing battery storage and possibly

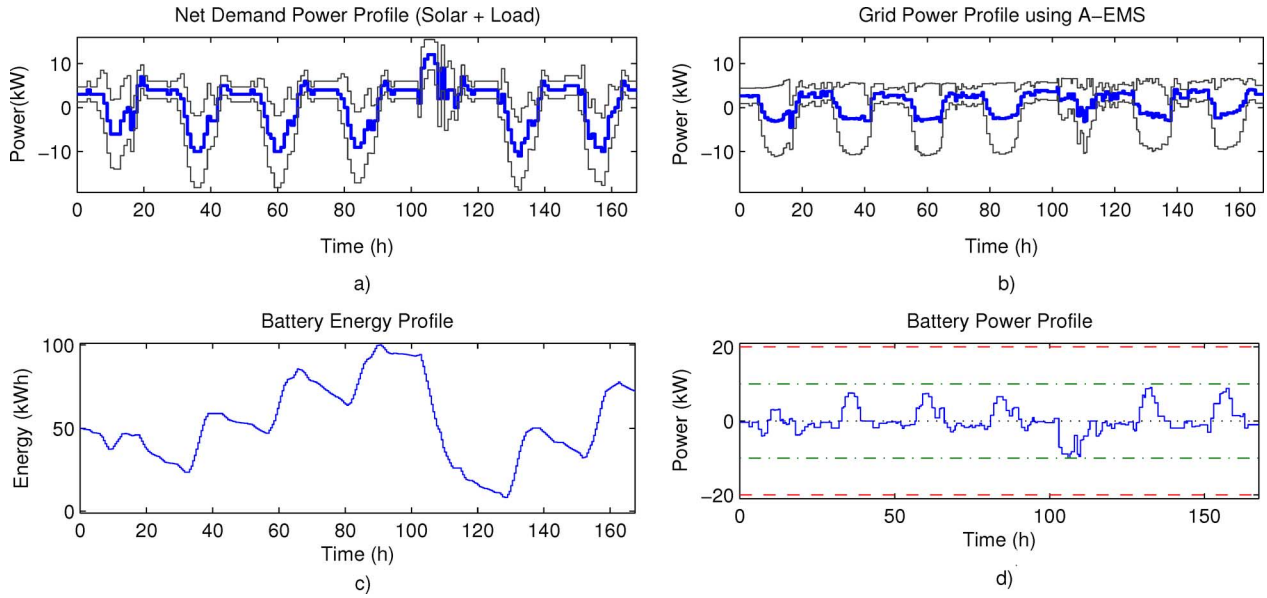


Fig. 10. Smoothing of solar with load power profile using 100 kWh battery. (a) Predicted net demand power profile. (b) Grid power profile with A-EMS. (c) Battery energy profile. (d) Battery power profile. Note in (a) and (b) the thin black lines indicate the upper and lower bounds.

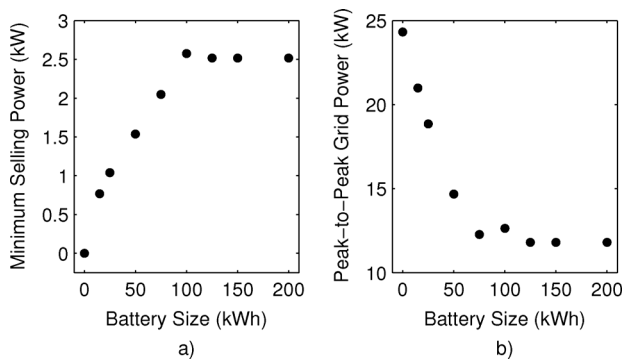


Fig. 11. Effect of battery size on flattening of solar power profile. (a) Minimum selling power, equal to $|p_g^{\max}|$. (b) Peak-to-peak fluctuation of grid power signal, equal to $p_g^{\max} - p_g^{\min}$.

renewable energy sources such as solar and wind power. The controllers make use of predicted net energy demand to fulfill multiple objectives. These objectives can be customized by the system user and range from economic savings to battery/grid signal shaping. The optimization problem was formulated with computation cost in mind to allow for system implementation on cost-effective embedded computer platforms. Speed improvements arise from utilizing variable time step lengths and binary constraint relaxations. The concept of battery incremental red-zone power rates has also been proposed as a means to enhance battery management. A robust variation of the controller was also proposed to handle uncertainty in the prediction of demand and local renewable power generation, with a very modest increase in the computations. The robust formulation of the optimization maintained its MILP structure, and therefore is computationally more efficient than many other robust optimization approaches. Simulation results with real data were presented to demonstrate the effectiveness of various features of the proposed controller.

A number of problems will be studied in future. These include load scheduling, e.g., for electric vehicle charging, algorithms for the prediction of demand and renewable power, and A-EMS for islanding mode operation. Alternative robust optimization approaches will also be explored.

## ACKNOWLEDGMENT

The authors would like to acknowledge Dr. Tim Davidson (Department of Electrical and Computer Engineering, McMaster University) for his guidance on robust optimization, and Burlington Hydro Inc. (Burlington, Ontario, Canada) for providing the electrically usage and solar power production data.

## REFERENCES

[1] X. Wang, J. M. Guerrero, F. Blaabjerg, and Z. Chen, "A review of power electronics based microgrids," *J. Power Electron.*, vol. 12, no. 1, pp. 181–192, 2012.
[2] R. Zamora and A. K. Srivastava, "Controls for micro grids with storage: Review, challenges, and research needs," *Renew. Sustain. Energy Rev.*, vol. 14, no. 7, pp. 2009–2018, 2010.
[3] A. Ravichandran, P. Malysz, S. Sirouspour, and A. Emadi, "The critical role of microgrids in transition to a smarter grid: A technical review," in *Proc. IEEE Transport. Electrificat. Conf. and Expo (ITEC)*, 2013, pp. 1–7, IEEE.
[4] Q. Deng, X. Gao, H. Zhou, and W. Hu, "System modeling and optimization of microgrid using genetic algorithm," in *Proc. 2nd Int. Conf. Intell. Control Inf. Process.*, 2011, pp. 540–544.
[5] F. A. Mohamed and H. N. Koivo, "Online management of microgrid with battery storage using multiobjective optimization," in *Proc. Int. Conf. Power Eng, Energy Elect. Drives*, 2007, pp. 231–236.
[6] Y. Levron, J. M. Guerrero, and Y. Beck, "Optimal power flow in microgrids with energy storage," *IEEE Trans. Power Syst.*, vol. 28, no. 3, pp. 3226–3234, Aug. 2013.
[7] A. A. Moghaddam, A. Seifi, T. Niknam, and M. R. A. Pahlavani, "Multi-objective operation management of a renewable mg (micro-grid) with back-up micro-turbine/fuel cell/battery hybrid power source," *Energy*, vol. 36, no. 11, pp. 6490–6507, 2011.
[8] S. Mohammadi, B. Mozafari, S. Solimani, and T. Niknam, "An adaptive modified firefly optimisation algorithm based on hong's point estimate method to optimal operation management in a microgrid with consideration of uncertainties," *Energy*, vol. 51, no. 1, pp. 339–348, 2013.
[9] H. Kim and T. Kinoshita, "A new challenge of microgrid operation," *Comm. Comp. Info Sci.*, vol. 78, pp. 250–260, 2010.
[10] S. Chakraborty, M. D. Weiss, and M. G. Simões, "Distributed intelligent energy management system for a single phase high-frequency ac microgrid," *IEEE Trans. Ind. Electron.*, vol. 54, no. 1, pp. 97–109, Feb. 2007.

[11] H. Morais, P. Kádár, P. Faria, Z. A. Vale, and H. M. Khodr, "Optimal scheduling of a renewable micro-grid in an isolated load area using mixed-integer linear programming," *Renewable Energy*, vol. 35, no. 1, pp. 151–156, 2010.
[12] A. G. Tsikalakis and N. D. Hatziargyriou, "Centralized control for optimizing microgrids operation," *IEEE Trans. Energy Conversion*, vol. 23, no. 1, pp. 241–248, Mar. 2008.
[13] A. Chaouachi, R. Kamel, R. Andoulsi, and K. Nagasaka, "Multiobjective intelligent energy management for a microgrid," *IEEE Trans. Ind. Electron.*, vol. 60, no. 4, pp. 1688–1699, Apr. 2013.
[14] E. Handschin, F. Neise, H. Neumann, and R. Schultz, "Optimal operation of dispersed generation under uncertainty using mathematical programming," *Int. J. Elect. Power Energy Syst.*, vol. 28, no. 9, pp. 618–626, 2006.
[15] A. Ulbig, M. Arnold, S. Chatzivasileiadis, and G. Andersson, "Framework for multiple time-scale cascaded mpc application in power systems," in *Proc. 18th IFAC World Congr.*, 2011, pp. 10472–10480.
[16] A. Molderink, V. Bakker, M. Bosman, J. Hurink, and G. Smit, "On the effects of mpc on a domestic energy efficiency optimization methodology," in *Proc. IEEE Int. Energy Conf.*, 2010, pp. 120–125.
[17] T. G. Hovgaard, L. F. S. Larsen, and J. B. Jørgensen, "Robust economic mpc for a power management scenario with uncertainties," in *Proc. IEEE Conf. Dec. Control Eur. Cont. Conf.*, 2011, pp. 1515–1520.
[18] A. Parisio and L. Glielmo, "Energy efficient microgrid management using model predictive control," in *Proc. IEEE Conf. Dec. Control Euro. Cont. Conf.*, 2011, pp. 5449–5454.
[19] D. L. Peters, A. R. Mechtenberg, J. Whitefoot, and P. Y. Papalambros, "Model predictive control of a microgrid with plug-in vehicles: Error modeling and the role of prediction horizon," in *Proc. ASME Dynamic Syst. Control Conf.*, 2011, pp. 1–8.
[20] J. Bendtsen, K. Trangbaek, and J. Stroustrup, "Hierarchical model predictive control for resource distribution," in *Proc. IEEE Conf. Dec. Control*, 2010, pp. 2468–2473.
[21] Z. Li, R. Ding, and C. A. Floudas, "A comparative theoretical and computational study on robust counterpart optimization: I. Robust linear optimization and robust mixed integer linear optimization," *Ind. Eng. Chem. Res.*, vol. 50, no. 18, pp. 10567–10603, 2011.
[22] N. Megiddo, "On the complexity of linear programming," *Adv. in Econ. Theory*, pp. 225–268, 1987.
[23] "Electricity prices for residential consumers," Jan. 2012 [Online]. Available: http://ieso.ca/imoweb/siteShared/options.asp?sid=ic

**Pawel Malysz** (S'06–M'12) received the B.Eng. degree in engineering physics and the M.A.Sc. and Ph.D. degrees in electrical engineering from McMaster University, Hamilton, ON, Canada, in 2005, 2007 and 2011, respectively.

In 2003–2004, he was a Biomedical Engineering Intern at the Juravinski Cancer Centre, Hamilton, ON, Canada. He is currently a Principal Research Engineer at the McMaster Institute for Automotive Research and Technology, a Canada Excellence Research Centre. His research interests include energy systems, battery management software design, haptics, robotics, and advanced control engineering.

**Shahin Sirouspour** (S'00–M'04) received the B.Sc. and M.Sc. degrees in electrical engineering from Sharif University of Technology, Tehran, Iran, in 1995 and 1997, respectively, and the Ph.D. degree in electrical engineering from the University of British Columbia, Vancouver, BC, Canada, in 2003.

He then joined McMaster University, Hamilton, ON, Canada, where he is currently an Associate Professor in the Department of Electrical and Computer Engineering. His research interests include teleoperation control, haptics, medical robotics, medical image processing, and smart grid/microgrid. He was on research leave at MDA Space Missions (Brampton, ON, Canada) during the period July 2010–June 2011.

Dr. Sirouspour received the McMaster President's Award of Excellence in Graduate Supervision in 2008.

**Ali Emadi** (S'98–M'00–SM'03–F'13) is the Canada Excellence Research Chair in Hybrid Powertrain and Director of McMaster Institute for Automotive Research and Technology (MacAUTO) at McMaster University in Hamilton, ON, Canada. Before joining McMaster University, he was the Harris Perlstein Endowed Chair Professor of Engineering and Director of the Electric Power and Power Electronics Center and Grainger Laboratories at Illinois Institute of Technology (IIT) in Chicago, IL, USA. In addition, he was the Founder, Chairman, and President of Hybrid Electric Vehicle Technologies, Inc. (HEVT) a university spin-off company of IIT. He is the recipient of numerous awards and recognitions. He was the advisor for the Formula Hybrid Teams at IIT and McMaster University, which won the GM Best Engineered Hybrid Systems Award at the 2010 and 2013 competitions, respectively. He is the principal author/coauthor of over 300 journal and conference papers as well as several books including *Vehicular Electric Power Systems* (CRC, 2003), *Energy Efficient Electric Motors* (CRC, 2004), Uninterruptible Power Supplies and Active Filters (CRC, 2004), *Modern Electric, Hybrid Electric, and Fuel Cell Vehicles, Second Edition* (CRC, 2009), and *Integrated Power Electronic Converters and Digital Control* (CRC, 2009). He is also the editor of the *Handbook of Automotive Power Electronics and Motor Drives* (CRC, 2005).

Dr. Emadi was the inaugural general chair of the 2012 IEEE Transportation Electrification Conference and Expo (ITEC) and has chaired several IEEE and SAE conferences in the areas of vehicle power and propulsion.